

MATNet: Multi-Level Fusion Transformer-Based Model for Day-Ahead PV Generation Forecasting

Matteo Tortora, *Graduate Student Member, IEEE*, Francesco Conte, *Senior Member, IEEE*, Gianluca Natrella, Paolo Soda, *Member, IEEE*

Abstract—Accurate forecasting of renewable generation is crucial to facilitate the integration of Renewable Energy Sources (RES) into the power system. Focusing on photovoltaic (PV) units, forecasting methods can be divided into two main categories: physics-based and data-based strategies, with Artificial Intelligence (AI)-based models providing state-of-the-art performance. However, while these AI-based models can capture complex patterns and relationships in the data, they ignore the underlying physical prior knowledge of the phenomenon. Therefore, in this paper we propose MATNet, a novel self-attention transformer-based architecture for multivariate multi-step day-ahead PV power generation forecasting. It consists of a hybrid approach that combines the AI paradigm with the prior physical knowledge of PV power generation of physics-based methods. The model is fed with historical PV data and historical and forecast weather data through a multi-level joint fusion approach. The effectiveness of the proposed model is evaluated using the Ausgrid benchmark dataset with different regression performance metrics. The results show that our proposed architecture significantly outperforms the current state-of-the-art methods. These findings demonstrate the potential of MATNet in improving forecasting accuracy and suggest that it could be a promising solution to facilitate the integration of PV energy into the power grid.

Index Terms—Forecasting, Multimodal Learning, Photovoltaic Generation, Renewable Energy Source, Transformer.

I. INTRODUCTION

Given the combination of climate change and the consequent need to reduce greenhouse gas emissions, the integration of renewable energy into power systems is steadily increasing. The shift towards RESs is crucial to a sustainable, affordable, accessible, clean, and low-carbon future, reducing polluting emissions and dependence on fossil fuels. In this regard, PV energy certainly is one of the most mature RES technologies, called to play a crucial role in accomplishing various climate protection goals [1]–[3].

Compared to fossil fuel-derived energy, green energies are substantially more sustainable. However, their inherent intermittent nature does not guarantee constant production flows, causing imbalances in the power system that ultimately limit

large-scale adoption [4], [5]. PV energy generation forecasting could help resolve these imbalances and uncertainties, facilitating the general integration of RES into the power systems [5]–[9]. Therefore, accurate forecasting of PV production emerges as an essential stakeholder to realise the full potential of PV systems and provide grid operators and energy traders with valuable insights and decision-making information to optimise maintenance strategies, plan the development of new plants, mitigate operational and management challenges, and improve economic returns on investment [6], [10]–[12].

For this reason, several methods for forecasting PV energy production have recently been developed. Currently, PV forecasting methods can be divided into two main categories: physics-based and data-based strategies. The latter can be further split into statistics-based and AI-based methods.

Physical-based methods, also known as Numerical Weather Prediction (NWP), are mathematical models that simulate complex systems to predict how the atmosphere will evolve. These models are based on fluid dynamics and thermodynamic principles and use a combination of observations from weather stations, satellites, radars, and other sources to predict atmospheric dynamics. However, these methods have certain limitations. The main drawback of these approaches is their lack of flexibility, as they require intensive knowledge about the considered phenomena and can be expensive in terms of time and resources. Additionally, they require extensive computer resources to run effectively [6], [13].

On the other hand, statistical methods include well-known approaches like linear regression, Auto Regressive Moving Average or Auto-Regressive Integrated Moving Average. These methods are mainly used to determine the mathematical relations in data, assuming linear models. Despite their widespread use in the literature, they are unsuitable for discovering non-linear relations, and their forecast accuracy depends heavily on the available data quality and size [10].

Due to their ability to discover complex relations, deal with unstructured data, and superior performance, AI-based models have focused the research in recent years. Compared with the above methods, they allow for easier modelling without requiring prior knowledge of the phenomenon's dynamics [14]. In particular, the Deep Learning (DL) paradigm can potentially boost performance significantly due to its ability to generalise and automatically extract abstract representations. Among these methods, recurrent neural networks (RNNs) and convolutional neural networks (CNNs) are the most used DL-based architecture providing state-of-the-art performance in PV power forecasting [8].

Manuscript received x x, xxxx; revised x x, xxxx. (*Corresponding author: Francesco Conte.*)

M. Tortora and P. Soda are with the Unit of Computer Systems & Bioinformatics Department of Engineering, University Campus Bio-Medico of Rome Via Alvaro del Portillo 21, 00128 Rome, Italy (e-mail: m.tortora@unicampus.it; p.soda@unicampus.it).

F. Conte is with the Unit of Innovation, Entrepreneurship & Sustainability, Department of Engineering, University Campus Bio-Medico of Rome Via Alvaro del Portillo 21, 00128 Rome, Italy (e-mail: f.conte@unicampus.it).

G. Natrella is with the DITEN, University of Genoa, Via all'Opera Pia 11a, Genoa, 16145, Italy (e-mail: gianluca.natrella@edu.unige.it).

In PV systems, the amount of energy produced is heavily influenced by weather factors, such as solar radiation. While DL methods have shown promising results in forecasting PV energy production, they ignore the underlying physical prior knowledge of the phenomenon. This is where NWP-based methods can be incredibly advantageous, as they provide valuable insights about the weather factors that affect energy production and, therefore, can help improve forecasting accuracy. Despite the potential benefits, relatively few works have explored the combination of NWP and DL models [14], [15].

Hence, in this work we propose MATNet, a novel self-attention-based architecture for multi-step day-ahead PV power production forecasting, combining the advantages of a DL approach with the a priori knowledge of the phenomenon provided by physical-based models.

The contributions of this work are summarised as follows:

- We propose a novel self-attention transformer-based architecture for multivariate multi-step day-ahead PV generation forecasting. The attention mechanism is a vital part of the architecture enabling the model to focus on input data elements dynamically.
- The proposed architecture consists of a hybrid approach that combines the ability to generalise and automatically capture complex patterns and relations in the data, typical of the DL paradigm, with the prior physical knowledge of PV energy generation of NWP methods. By combining these two approaches, our model can achieve a more accurate and robust PV generation forecast.
- We fed the proposed model with historical PV data and historical and forecast weather data. The historical and forecast weather data are conceptually different as they observe the phenomenon at different points in time. Therefore, the architecture handles these input branches through joint fusion performed at different levels of abstraction.
- We propose a dense interpolation module to simplify the high-dimensional representation returned by the attention-based module.
- We evaluate the model's effectiveness by comparing it extensively with the Ausgrid benchmark dataset [16], using different regression performance metrics and ablation studies.

The rest of this manuscript is organised as follows: [Section II](#) presents a review of related work. [Section III](#) introduces the dataset, overviewing the pre-processing adopted. [Section IV](#) describes the details of our approach, whilst [Section V](#) describes the experimental setup and discusses the results. Finally, [Section VI](#) provides concluding remarks.

II. RELATED WORK

This section will focus only on work related to the Ausgrid dataset [16]. It contains the historical individual energy production data of 300 residential PV solar units. In [Section III-A](#), we will analyse this dataset in further detail.

In [17] the authors proposed an ensemble approach for 24-hours-ahead PV generation forecasting. The idea behind this is to break down the PV production time series into

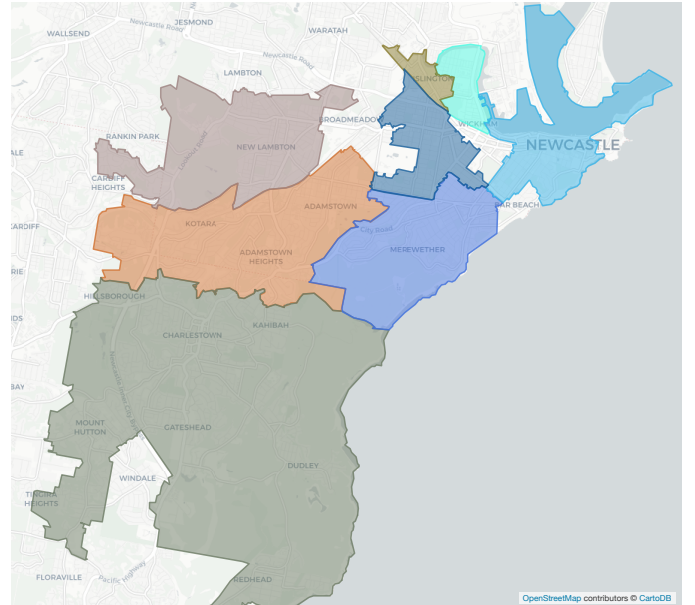


Figure 1. Map of the territorial areas containing the 26 PV units considered in this study, generated using the PyTrack library [20]. Each coloured area corresponds to a distinct geographical region associated with one of the eight zip codes.

sub-time sequences, so that each of these sub-time series collects PV power records for the same time and all days of the year, creating a time series for every 30 minutes of production. Therefore, their approach consists of an ensemble of simple univariate models based on Least Squares Support Vector Regression, each of which predicts the PV output of each 30 minutes of the following day. The authors validated their approach using the dataset provided by Ausgrid. They demonstrated that the proposed approach is generic and any machine learning algorithm for regression can be used. Despite the model giving good results for *clear* and *partly cloudy* days, it fails to handle the *cloudy/overcast* type of day.

In [18] the authors proposed a novel Bayesian probabilistic technique for forecasting renewable power production addressing data and model uncertainties by integrating bi-directional short-term memory (BiLSTM) neural networks while compressing high dimensionality presented in weights' parameters with a variational autoencoder. Also for this work, the authors validated their method using the publicly available PV power database provided by Ausgrid. Early results show how their approach outperforms other probabilistic DL methods regarding forecasting accuracy. The same authors in [19] proposed an improved Bayesian BiLSTM-based DL technique for multi-step ahead PV generation forecasting applying an alpha-beta divergence for a more appropriate consideration of outliers. The proposed method is evaluated using the PV generation data provided by Ausgrid. The results demonstrate that the improved Bayesian BiLSTM with alpha-beta divergence outperforms standard Bayesian BiLSTM and other benchmark methods for multi-step ahead forecasting in terms of lower error values.

III. MATERIALS

In this work, we utilise three primary data sources for multi-step PV power production forecasting: Ausgrid, OpenWeatherMap, and Solcast. Ausgrid is the electricity distributor for New South Wales, Australia, and provides a dataset on historical electricity demand and PV power generation. OpenWeatherMap is an online weather data service that provides real-time, forecast, and historical weather data. Lastly, Solcast is an online solar data service providing forecasts, live and historical solar irradiance, as well as weather data. It is freely available for public research purposes or implementation in household systems. In the following, we will describe in further detail the characteristics and features of these datasets, as well as the pre-processing steps used in this study.

A. Ausgrid

In this work, we utilised as the primary source of data the “Solar home electricity dataset” provided by Ausgrid [16]. This distribution network service provider owns, maintains, and operates the electricity distribution network in Sydney, the Central Coast, and the Hunter regions of New South Wales, Australia. The dataset contains power generation (in kWh) for 300 residential rooftops solar PV units recorded directly from the PV inverter over the period from 1 July 2010 to 30 June 2013 with a sampling time of 30 minutes. In addition to PV generation, where each entry represents the power produced by the PV unit in the previous half hour, the dataset contains also the following information:

- Installed solar panel capacity for each of the 300 PV units (in kilowatt-peak kWp). This represents the PV panels’ peak power under full solar radiation and tested under standard conditions.
- Total consumption (in kWh) at all times, not including power generated by solar sources and controlled load supply.
- Postal code location of the customer, for a total of 100 unique postal codes.

In this work, we focused solely on PV energy generation data. To ensure data integrity, we selected only 26 out of 300 households with PV units spread over a 75-square-kilometre area and located in 8 different zip codes within the Newcastle region, as illustrated in Figure 1. A comprehensive list of the included customers can be found in Appendix A.

We pre-processed the data in multiple steps. First, we subsampled the time series at an hourly sampling frequency aggregating the PV power generated during the previous hour. Then, each entry was normalised between 0 and 1 by dividing it by the peak power of the relative generator:

$$\hat{p}_{i,s} = \frac{p_{i,s}}{P_s},$$

where $p_{i,s}$ is the production value at time step i for the s -th PV unit, and P_s is the peak power for PV unit s . Finally, we aggregated the PV facilities’ historical data averaging each entry by timestamps to get a comprehensive overview. Samples are generated using a sliding window process parameterised by two parameters: the width of the sliding block (w_{length})

Table III.1
WEATHER ATTRIBUTES EXTRACTED FROM OPENWEATHER API AND SOLCAST.

Attribute	UoM	Description
Temperature	K	Temperature
Feels like	K	Human perception of weather temperature
Pressure	hPa	Atmospheric pressure (on the sea level)
Humidity	%	Humidity
Dew point	K	Temperature at which condensation occurs
Wind speed	m s^{-1}	Wind speed
Wind deg	deg	Wind direction
Wind gust	m s^{-1}	Wind gust
Clouds all	%	Cloudiness
Rain 1h	mm	Rain volume for the last hour
Weather description	-	Categorical weather conditions
Direct Normal Irradiance (DNI)	W m^{-2}	Direct Normal Irradiance
Diffuse Horizontal Irradiance (DHI)	W m^{-2}	Diffuse Horizontal Irradiance
Global Horizontal Irradiance (GHI)	W m^{-2}	Global Horizontal Irradiance

and the distance between each window ($step$). These samples are used to make predictions for the following 24-hour time steps.

B. Weather Conditions

In this study, we utilised as the primary source for meteorological data OpenWeatherMap service [21]. It provides weather data for any location using an NWP proprietary model. It is fed with 82,000 weather stations spread globally, radars, and weather satellites.

In addition to the meteorological data obtained from OpenWeatherMap, we have incorporated solar radiation data from Solcast [22]. These measurements include:

- DNI: It represents the direct irradiance received on a surface held perpendicular to the sun, providing information about solar radiation intensity when the sunlight reaches the surface directly without any obstructions.
- DHI: It refers to the diffuse irradiance received on a horizontal surface. It quantifies the scattered radiation caused by atmospheric factors such as clouds, haze, and pollution.
- GHI: This measurement represents the irradiance received on a horizontal surface. It takes into account both direct sunlight and diffuse sky radiation and is crucial for assessing the overall solar energy potential of a location.

By incorporating Solcast’s DNI, GHI and DHI data, we obtain a more in-depth insight into the availability and intensity of solar energy at the specified location.

Table III.1 describes the climate attributes provided by both the OpenWeatherMap API and Solcast considered in this work. Unlike all other variables which are numerical features, the *weather description* attribute is a categorical feature with 22 distinct levels, listed in depth in Appendix B. In order to convert these categorical values into numeric ones we apply a one-hot encoding, as no ordinal relation exists for these variables.

As for the power production data, we generated samples through a sliding window process. Since both OpenWeatherMap API and Solcast do not provide historical weather forecast data for the considered period, in this work, we simulate the weather forecast for the following 24-hour time steps using the actual historical weather data. At the end of this

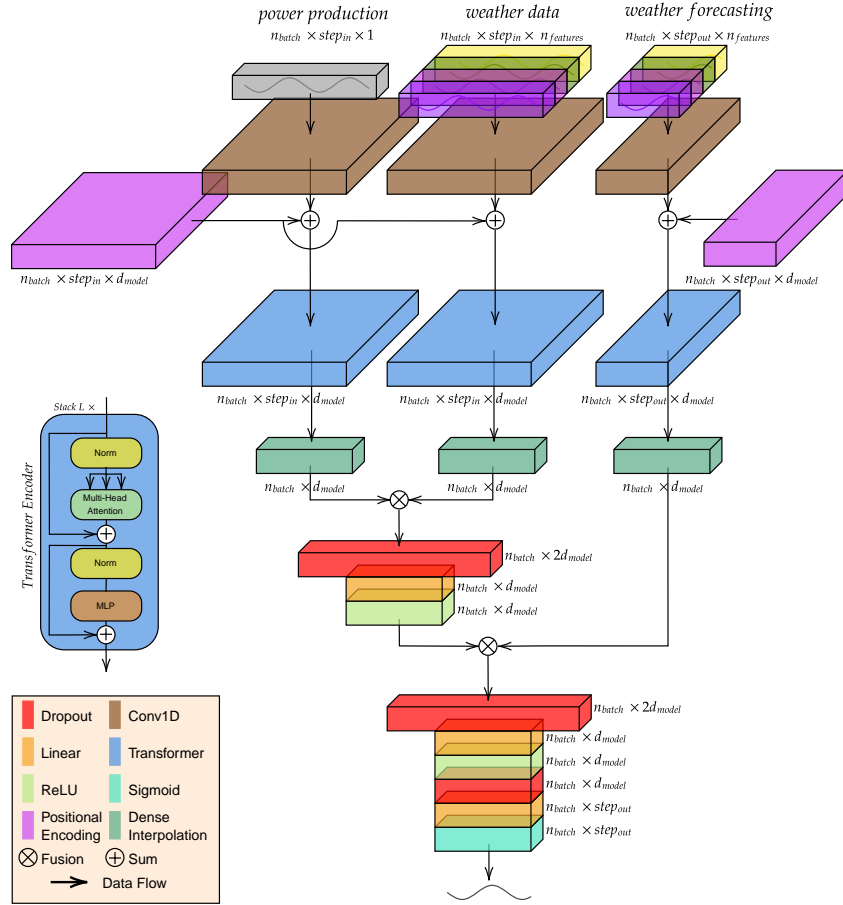


Figure 2. Overall architecture of our proposed MATNet.

pre-processing process for the meteorological data, we obtain a multivariate time series consisting of 35 attributes.

IV. PROPOSED ARCHITECTURE

This section presents MATNet, our multi-level fusion and self-attention transformer-based model for multivariate multi-step day-ahead PV forecasting, fed with historic PV production and historical and forecasted weather data. The proposed architecture is illustrated in Figure 2. In the following sections, we will delve into the specifics of each component and explain how they work together to achieve the desired outcome.

A. Embedding Module

Our architecture accepts as input a 3-tuple of multivariate time series of the type $\langle pv, hw, fw \rangle$, where $pv \in \mathbb{R}^{step_{in} \times 1}$, $hw \in \mathbb{R}^{step_{in} \times 35}$ and $fw \in \mathbb{R}^{step_{out} \times 35}$ represents the historical PV power production, the historical weather data and the forecast weather data of the next 24-hour time steps to be predicted, respectively. Hence, the first step in our architecture is an embedding module that maps the multivariate time series into a high-dimensional representation space to facilitate the sequence modelling. Hence, in this work, we implement a 1D

convolutional layer as an embedding module to project the input data to a d_{model} -dimensional space:

$$\mathbf{o}_i = \mathbf{b}_i + \sum_{k=0}^{C_{in}-1} \mathbf{w}_{i,k} * \mathbf{in}_{i,k} \quad \forall i \in \{0, \dots, C_{out}-1\}$$

where $\mathbf{w} \in \mathbb{R}^{1 \times size}$ is the convolution kernel, C_{in} and C_{out} are the input and the output channels, \mathbf{b} is the bias term, $*$ is the sliding dot product operator.

When working with PV production data ($C_{in} = 1$), the convolutional layer uses a kernel with a size of 3 to capture patterns across the temporal dimension. However, when analysing weather data ($C_{in} = 35$), we use a kernel size of 1, allowing the convolutional layer to focus on capturing dependencies across different time series attributes without considering temporal information. In both cases, the number of output channels is set to d_{model} .

In conclusion, the output of the embedding module produces multivariate time series with the same number of time steps as the input, but in a higher dimensional representation with d_{model} attributes. These higher dimensional representations are then used as input for an attention mechanism, to further improve the model performance.

B. Positional Encoding

As our architecture does not contain any recurrence, we include a positional encoding layer in order to incorporate the relative or absolute position of the time steps within the input-embedded sequence. This is particularly important for sequential data, as the ordering of the elements can carry valuable information allowing the model to better capture the temporal dependencies in the data and improve the performance of the network.

In this work, we use sine and cosine functions of different frequencies as in [23]:

$$\vec{p}_t^{(i)} := \begin{cases} \sin \omega_k \cdot t, & \text{if } i = 2k \\ \cos \omega_k \cdot t, & \text{if } i = 2k + 1 \end{cases},$$

where:

$$\omega_k = \frac{1}{10000^{\frac{2k}{d_{model}}}}$$

and $\vec{p}_t^{(i)}$ represents the positional encoding for the t -th time step in the input sequence along the i -th dimension, and d_{model} is the input embedding dimension. The d_{model} -dimensional positional embedding is then added to the input embedding since they share the same dimension. Note that, there are many choices for positional encodings, such as randomised lookup tables or learnable representations [24].

C. Self-Attention

Our MATNet architecture relies on self-attention mechanisms to process sequential input data. Self-attention, also known as intra-attention, allows the model to attend to different parts of the whole input sequence, weighing the importance of each component at each position. Unlike recurrent layers that process input data sequentially using recurrent connections and maintaining hidden states to propagate information through time, the self-attention mechanism processes the input sequence in parallel and weighs the importance of each element independently [23], [25].

An attention function maps a query and a set of key-value pairs to an output. In this work, we used the self-attention mechanism as proposed in [23], where the attention mechanism is represented as:

$$\text{Attention}(\mathbf{Q}, \mathbf{K}, \mathbf{V}) = \text{softmax}\left(\frac{\mathbf{Q}\mathbf{K}^T}{\sqrt{d_{model}}}\right)\mathbf{V}$$

where d_{model} is the dimension of the key vectors, and \mathbf{Q} , \mathbf{K} and \mathbf{V} are all linear transformations of the input embedding with the added positional encodings. As proposed in the paper, we extended the attention mechanism using multi-head attention. Instead of performing a single attention function with keys, values, and queries d_{model} -dimensional matrices, these are linearly projected in h lower-dimensional sub-spaces. These h -projected representations fed the attention mechanisms in parallel, yielding d_v -dimensional output values allowing the model to attend to information from different representation sub-spaces at different positions. Each head can be interpreted to encode complementary details on different types

of temporal dependencies [26]. Finally, these are concatenated and linearly projected to obtain the final representation:

$$\text{MultiHead}(Q, K, V) = \text{Concat}(\text{head}_1, \dots, \text{head}_h) W^O$$

where $\text{head}_i = \text{Attention}\left(QW_i^Q, KW_i^K, VW_i^V\right)$

where $W_i^Q \in \mathbb{R}^{d_{model} \times d_k}$, $W_i^K \in \mathbb{R}^{d_{model} \times d_k}$, $W_i^V \in \mathbb{R}^{d_{model} \times d_v}$, and $W^O \in \mathbb{R}^{hd_v \times d_{model}}$ represents the projections matrices for i -th head and for the output, respectively. In this work, we use the same dimension for the queries, keys and values $d_k = d_v = d_{model}/h$.

The second block of the attention module is a simple feed-forward block downstream of the multi-headed attention layer. Besides, a normalisation layer is applied before every block, whilst residual connections are after every block [27], [28].

This attention module is stacked L times, and the final representations of the entire sequence are obtained from the final attention one. We then use a dense interpolated embedding technique to simplify and create a concise representation.

D. Dense Interpolation Layer

Unlike recurrent layers that produce a hidden state summarising the information from the entire multivariate input sequence [25], the attention-based module returns a high-dimensional representation. Hence, we need to add a dense interpolation embedding layer to simplify and produce a concise representation while capturing temporal structure and preserving temporal order. In this work, we implement a dense interpolation layer inspired by an interpolation algorithm from language modelling [29] also used to deal with time-series data [26]. The idea is to interpolate the representation from the attention module, weighting the hidden representation's contribution $\mathbf{s}_t \in \mathbb{R}^{d_{model}}$ at time step t , by a factor:

$$w = \left(1 - \frac{|s - m|}{M}\right)^2$$

where s is the relative position of time step t in the final representation and m is the position in the final representation of length M . This is efficiently implemented performing the following matrix operation: $\mathbf{U} = \mathbf{S} \times \mathbf{W}$, where $\mathbf{S} = [\mathbf{s}_1, \dots, \mathbf{s}_T]$ and $\mathbf{W} \in \mathbb{R}^{T \times M}$ storing the weights w .

Inspired by this concept, we created a modified version of the module where the weights w are learned through the back-propagation process. Figure 3 shows a visual representation of the dense interpolation module. The edges are coloured based on the weight values of w , with darker edges showing a more decisive influence and lighter ones indicating a weaker impact. Finally, we can create a single, unified hidden representation in several ways. The easiest method is to concatenate the embeddings from each time step. In this work, we use the last embedding as the single hidden representation, which summarises the information from the entire input sequence through the aforementioned dense interpolation module.

E. Multi-Level Joint Fusion

The dense interpolation stage leads to the creation of three representation vectors in $\mathbb{R}^{d_{model}}$, each representing the

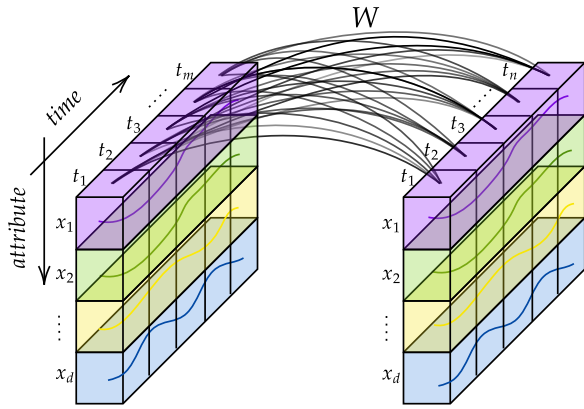


Figure 3. Visualising the dense interpolation module. Where m, n, d , are the length of the time series, the interpolation factor, and the number of time series attributes, respectively. In this work, we have that $m = step_{in}$, $d = d_{model}$ and $n = M$.

PV production history, weather history, and weather forecast branches, respectively. To combine these branch-specific representations into a multimodal vector, we use a fusion layer also known as a shared representation layer. There are several approaches proposed for joint fusion, such as summation, mean, Kronecker product, etc. However, the most widely used approach is concatenation, and so, we have adopted this approach in our work. For further information on this topic, please refer to [30].

The input branches are conceptually different as they observe the phenomenon at different points in time. Indeed, while the production history and weather data observe the history of the phenomenon, the weather forecasts observe the future and have a dimensionality equal to the number of timestamps to be predicted. To account for this, we use a multi-level fusion approach, fusing learned information from the previous stages at multiple levels of abstraction. Hence, since the two historical sequences (PV production and weather) are temporally correlated, we fused them at the first fusion level. The resulting vector is then processed through a fully connected module consisting of a dropout regularisation layer [31] and a dense layer with ReLU as an activation function. This hidden vector is then concatenated at a higher level of abstraction with the weather forecast representation from the dense interpolation layer. The joint representation is then fed to another fully connected module with a dropout layer and a dense layer with ReLU as an activation function. The final output module comprises a dropout layer and a linear layer with an output size equal to the number of timestamps to be predicted $step_{out}$ and with a Sigmoid activation function. In our case, we aim to predict the 24-hour PV production, so $step_{out} = 24$.

V. EXPERIMENTAL SETUP AND RESULTS

In this section, we present the experimental setup describing the training details and the evaluation metrics adopted. Then, we analyse the proposed MATNet model in several directions. First, we evaluate our model on the Ausgrid benchmark task and present a comparison with state-of-the-art and baseline

architecture based on recurrent layers. Then we verify the effectiveness of the proposed method through ablation studies.

A. Training Details

In this work, PV generation records from 1 July 2010 to 30 June 2012 are used as the training set, while the test set contains timestamps ranging from 1 July 2012 to 30 June 2013.

Unless otherwise specified, we use the following parameters for our architecture: input embedding dimensionality $d_{model} = 512$, parallel heads attention layers $h = 8$, number of sub-encoder-layers $L = 3$, the interpolation factor in the interpolation module $M = step_{in}$, time steps in the input sequence $step_{in} = 24$, time steps in the output sequence $step_{out} = 24$. We adopt a 24-hours time-horizon because the day-ahead prediction of renewable generation is the most common requirement of smart grid management algorithms (e.g. [32]–[35]), further considering the daily cyclical nature of PV generation.

Our proposed MATNet architecture and the entire training process are based on the PyTorch framework [36]. We trained all the models on a workstation with 1 NVIDIA A100 GPU for 200 epochs. The model weights and biases are updated using the Mean Squared Error (MSE) as a loss function, which measures the average squared difference between the predicted and the actual values. We used the Adam optimizer [37] with a learning rate of 10^{-3} and with β_1 and β_2 equal to 0.9 and 0.999, respectively. We reduced the learning rate throughout training by a factor of 0.2 once learning stagnates, and no improvement is seen for a patience number of epochs equal to 20. The code is publicly available on GitHub¹

B. Evaluation Metrics

We use the following evaluation metrics to assess the quality of the proposed forecast models:

- **Root Mean Squared Error:** it is calculated as the square root of the mean of the squared differences between the predicted and actual values:

$$RMSE = \sqrt{\frac{1}{n} \sum_{t=1}^n (y_t - \hat{y}_t)^2} \quad (1)$$

- **Mean Absolute Error:** it measures the average absolute difference between the predicted and actual values:

$$MAE = \frac{1}{n} \sum_{t=1}^n |y_t - \hat{y}_t| \quad (2)$$

- **Weighted Mean Absolute Percentage Error:** it measures the accuracy of a forecast, where the importance of the forecast errors is weighted according to the size of the actual values being forecast:

$$WMAPE = \frac{\sum_{t=1}^n |y_t - \hat{y}_t|}{\sum_{t=1}^n |y_t|} \quad (3)$$

¹The code is available at the following GitHub repository <https://github.com/cosbidev/MATNet>.

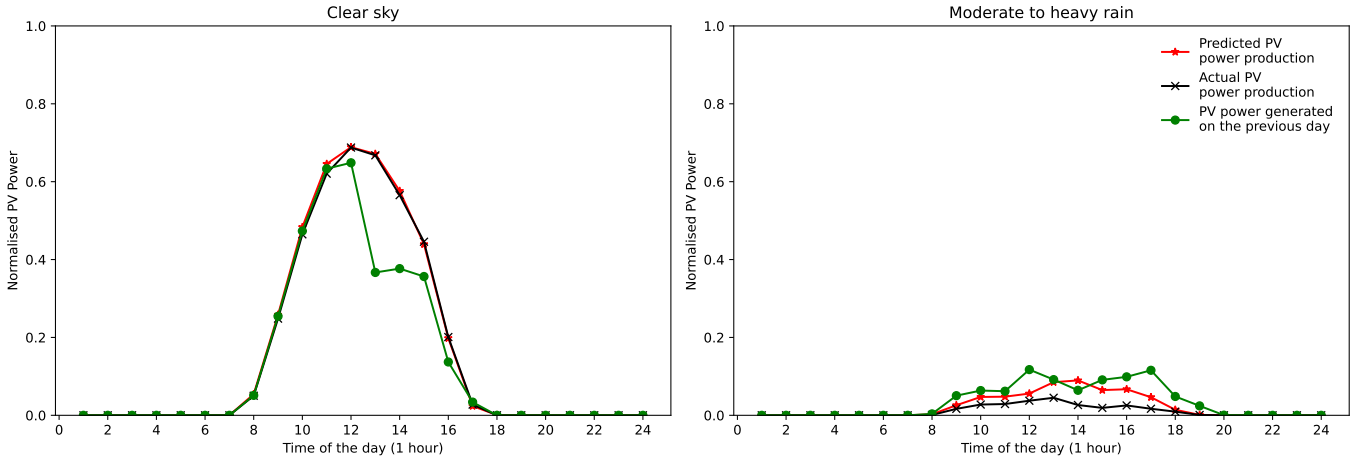


Figure 4. Forecasting results of MATNet on Ausgrid test set. On the left is the forecast for the best-performing day (2013-06-11), while on the right is the forecast for the worst-performing day (2013-01-28). Both predictions are evaluated using the MASE metric.

- **Mean Absolute Scaled Error:** it measures the accuracy of a forecast, where the forecast errors are scaled by the mean absolute error of a naïve forecast:

$$MASE = \frac{\frac{1}{n} \sum_{t=1}^n |y_t - \hat{y}_t|}{\frac{1}{n-1} \sum_{t=2}^n |y_t - y_{t-1}|} \quad (4)$$

In eqs. (1) to (4), n is the number of observations, y_i is the actual value of the i -th observation, and \hat{y}_i is the predicted value of the i -th observation. In all cases, lower values indicate more accurate forecasts.

C. Ausgrid Benchmark

This section offers a comparative analysis of the Ausgrid benchmark to assess the performance of MATNet with state-of-the-art methods [17]–[19]. It is worth noting that a completely direct comparison is not possible as no publicly available implementation of the methods was provided and that training and evaluation procedures were quite different. To offer a more in-depth analysis and a more direct comparison, in this section, we also compare our attention-based model with some recurrent-based baselines that share the same overall multi-level fusion MATNet architecture. These recurrent architectures share the same fusion and final fully connected layers, whilst the input embedding, positional encoding and dense interpolation modules are no longer necessary. Finally, instead of the attention layers, we use the Long-Short-Term Memory (LSTM), BiLSTM, Gated Recurrent Unit (GRU), and bi-directional GRU (BiGRU):

- LSTM is a recurrent neural network that uses gates to control the flow of information into and out of the cell state c_t [25]. The hidden state h_t at time step t is updated

as:

$$\begin{aligned} i_t &= \sigma(W_{ii}x_t + b_{ii} + W_{hi}h_{t-1} + b_{hi}) \\ f_t &= \sigma(W_{if}x_t + b_{if} + W_{hf}h_{t-1} + b_{hf}) \\ g_t &= \tanh(W_{ig}x_t + b_{ig} + W_{hg}h_{t-1} + b_{hg}) \\ o_t &= \sigma(W_{io}x_t + b_{io} + W_{ho}h_{t-1} + b_{ho}) \\ c_t &= f_t \odot c_{t-1} + i_t \odot g_t \\ h_t &= o_t \odot \tanh(c_t) \end{aligned}$$

where x_t is the input, σ is the sigmoid function, \odot is the Hadamard product, W and b are weights and biases, respectively, and i_t , f_t , g_t , o_t are the input, forget, cell, and output gates, respectively. BiLSTM is a variation of LSTM that processes input in both forward and backward directions.

- GRU is another recurrent network that uses gating mechanisms to control the flow of information between time steps [38]. The hidden state h_t at time step t is updated as:

$$\begin{aligned} r_t &= \sigma(W_{ir}x_t + b_{ir} + W_{hr}h_{t-1} + b_{hr}) \\ z_t &= \sigma(W_{iz}x_t + b_{iz} + W_{hz}h_{t-1} + b_{hz}) \\ n_t &= \tanh(W_{in}x_t + b_{in} + r_t \odot (W_{hn}h_{t-1} + b_{hn})) \\ h_t &= (1 - z_t) \odot n_t + z_t \odot h_{t-1} \end{aligned}$$

where r_t , z_t , and n_t are the reset, update, and new gates, respectively. Like BiLSTM, the BiGRU processes input in both forward and backward directions.

Finally, we compare the Dense Interpolation Layer proposed by [29] with our learnable version.

Table V.1 reports the performance in terms of RMSE, MAE, WMAPE, and MASE of our proposed model for the Ausgrid benchmark. As we can see, our proposed MATNet significantly outperforms the current state-of-the-art methods. As mentioned above, a direct comparison is impossible due to experimental setup differences. However, our method has been validated over a more extended test period and the reported metrics help to reduce possible differences by averaging the errors. For these reasons, we can make more meaningful

Table V.1

COMPARATIVE ANALYSIS OF THE PROPOSED METHOD FOR PV POWER PRODUCTION FORECASTING. BOLD FONT IS USED TO HIGHLIGHT THE BEST RESULTS FOR EACH METRIC. *NORMALISED MAE. †MATNET USING DENSE INTERPOLATION LAYER PROPOSED BY [29].

Architecture	RMSE	MAE	WMAPE	MASE
LsSVR [17]	-	4.95*	-	-
Bayesian BiLSTM [18]	0.0985	0.0679	-	-
Improved-Bayesian BiLSTM [19]	0.0854	0.0370	-	-
LSTM-based MATNet	0.0495	0.0267	0.1992	0.4709
GRU-based MATNet	0.0532	0.0291	0.2082	0.5003
BiLSTM-based MATNet	0.0540	0.0294	0.2107	0.5056
BiGRU-based MATNet	0.0533	0.0292	0.2047	0.4957
MATNet_wDIL [29] [†]	0.1333	0.0804	0.7357	1.6981
MATNet	0.0460	0.0245	0.1745	0.4177

comparisons and assert confidence in the validity of our model. Additionally, our attention-based architecture outperforms both our recurrent-based competitors and the MATNet version with the interpolation layer proposed by [29], and the differences were all statistically significant with a p -value less than 0.01, according to the Diebold-Mariano test [39]. These findings demonstrate the potential of MATNet in improving forecasting accuracy and suggest that it could be a promising solution for PV power production forecasting.

For the sake of completeness of the analysis, in Figure 4, we also show the PV production forecasts for the best-performing (left) and worst-performing (right) day according to the MASE metric. In black is the actual production curve and in red is the PV production forecast curve; besides, to provide additional context, we have also included the PV generation from the previous day, represented by the green curve. The plot on the left reveals the effectiveness of our MATNet on its best-performing day, with a MASE score equal to 0.0640. Predominantly clear skies characterise this day, and the forecast almost perfectly follows the actual PV production. On the other hand, the graph on the right shows the worst-performing day with a MASE equal to 3.2739. This is characterised by moderate to heavy rainfall throughout the day. Despite these conditions, the PV forecast still closely follows the trend of actual PV production but with a slightly different multiplication factor. This demonstrates the remarkable resilience and reliability of MATNet, which outperforms state-of-the-art methods that typically experience a decline in performance during adverse weather situations. The difference between the red (forecast) and green (previous day’s production) pattern also highlights that the forecast is not solely based on the previous day’s production, demonstrating the positive impact of incorporating weather forecasts in our model.

D. Ablation Study

MATNet is a highly versatile multimodal architecture incorporating heterogeneous input sources to improve performance. These inputs include PV production data, weather conditions, and weather forecasts. To understand the contribution of each input source, we conducted an ablation study. In this study, we systematically turned off each input branch to see how the model would perform without it. The results of this

Table V.2

ABLATION STUDY RESULTS FROM THE AUSGRID TEST SET COMPARING THE MATNET MODEL’S PERFORMANCE WITH VARIOUS INPUT BRANCHES DISABLED. BOLD FONT IS USED TO HIGHLIGHT THE BEST RESULTS FOR EACH METRIC.

PV Production	Weather History	Weather Forecast	RMSE	MAE	WMAPE	MASE
✓	✗	✗	0.1083	0.0626	0.5557	1.2985
✗	✓	✗	0.1143	0.0663	0.5172	1.2556
✗	✗	✓	0.0512	0.0275	0.1924	0.4639
✓	✓	✗	0.1005	0.0576	0.5552	1.2663
✓	✗	✓	0.0486	0.0261	0.1865	0.4445
✗	✓	✓	0.0488	0.0265	0.1876	0.4512
✓	✓	✓	0.0460	0.0245	0.1745	0.4177

analysis provide valuable insights into each input modality’s importance, helping us to assess the overall effectiveness of MATNet. To preserve the integrity of the architecture, we chose to turn off each modality by zeroing all the elements of the input branch, such as applying a 100% probability dropout layer. As a result, MATNet remains a highly versatile and robust solution, even when some modalities experience failures or lack data. This ensures that, in real-world scenarios, MATNet continue to operate effectively and reliably.

Table V.2 reports the results of the ablation analysis of MATNet in terms of RMSE, MAE, WMAPE and MASE. As might easily be expected, the version of MATNet with all three input channels (i.e., PV production, weather history and weather forecast) activated outperforms any other combination of input sources enabled, and the differences were all statistically significant with a p -value less than 0.01, according to the Diebold-Mariano test. These results further reinforce the concept that incorporating multiple heterogeneous data sources leads to a significant boost in the model’s overall performance. On the other hand, our results showed that the best-performing unimodal experiment was the one that used only weather forecasts. This highlights the crucial role that weather forecasts play in the overall performance of our model.

VI. CONCLUSIONS

In this work, we propose MATNet, a novel multimodal self-attention architecture for day-ahead, multi-step PV power generation forecasting. We feed the proposed architecture with historical PV data and historical and forecast weather data. Since they observe the phenomenon at different points in time, we use multi-level joint fusion to combine them at distinct abstraction levels.

Our work significantly outperforms the current state-of-the-art demonstrating the potential of MATNet to forecast day-ahead PV generation, even under challenging weather conditions. While our proposed method reaches remarkable results, it leverages a combination of forecast and historical weather data to improve the accuracy of PV production predictions. It is worth recognising that the acquisition of these data can involve costs in some cases. However, it is worth noting that the services utilised in our research provide access to these data free of charge for household PV systems. Therefore, incorporating meteorological data does not impose

any financial burden for the specific use case of household applications.

To further improve the proposed method by making it more resilient, robust and reliable, future work is directed towards developing an adaptive joint fusion layer. The idea is to dynamically weight the contribution of the various input branches to provide more weight to the weather forecast branch during adverse conditions. In this way, the model can better adjust its predictions to follow the typical silhouette of PV generation in clear weather, while giving more weight to the branch of the weather forecast in case of adverse conditions. Besides, another worthy future direction is the incorporation of the explainable AI paradigm into the proposed framework. By making the proposed framework interpretable, we can facilitate the integration of AI-based RES into the power systems, enabling energy stakeholders to make informed evidence-based decisions.

ACKNOWLEDGMENTS

This work was partially supported by POR FESR Lazio 2014-2020 under project no. A0375-2020-36770, and by PNRR MUR project PE0000013-FAIR. We also acknowledge partial support from Project ECS 0000024 Rome Technopole, - CUP C83C22000510001, NRP Mission 4 Component 2 Investment 1.5, Funded by the European Union - NextGenerationEU.

APPENDIX A

SELECTED AUSGRID CUSTOMERS

In this work, we only focused on 26 out of the 300 customers: 33, 47, 73, 87, 88, 110, 124, 144, 151, 153, 157, 163, 175, 176, 188, 200, 201, 207, 222, 240, 256, 259, 263, 272, 281, 293, for a total of 8 postal codes in Newcastle region. These have no missing values or artefacts due to inactivity, failures or interruptions.

APPENDIX B

WEATHER DESCRIPTION OF OPENWEATHERMAP

The following lists the various levels of the categorical *Weather Description* feature provided by the OpenWeatherMap API: *scattered clouds, few clouds, broken clouds, overcast clouds, sky is clear, light rain, thunderstorm, moderate rain, fog, light intensity shower rain, mist, haze, heavy intensity rain, light intensity drizzle, shower rain, smoke, thunderstorm with rain, proximity squalls, very heavy rain, light intensity drizzle rain, rain and drizzle, drizzle.*

REFERENCES

- [1] International Renewable Energy Agency, "Solar energy," 2020, [Online; accessed 2023-02-20]. [Online]. Available: <https://www.irena.org/Energy-Transition/Technology/Solar-energy>
- [2] International Energy Agency, "Solar-PV," 9 2022, [Online; accessed 2023-02-20]. [Online]. Available: <https://www.iea.org/reports/solar-pv>
- [3] Y. Zhou, "Artificial intelligence in renewable systems for transformation towards intelligent buildings," *Energy and AI*, p. 100182, 2022.
- [4] R. Meenal, D. Binu, K. Ramya, P. A. Michael, K. Vinoth Kumar, E. Rajasekaran, and B. Sangeetha, "Weather forecasting for renewable energy system: a review," *Archives of Computational Methods in Engineering*, vol. 29, no. 5, pp. 2875–2891, 2022.
- [5] J. Simeunović, B. Schubnel, P.-J. Alet, and R. E. Carrillo, "Spatio-temporal graph neural networks for multi-site pv power forecasting," *IEEE Transactions on Sustainable Energy*, vol. 13, no. 2, pp. 1210–1220, 2021.
- [6] C. Wan, J. Zhao, Y. Song, Z. Xu, J. Lin, and Z. Hu, "Photovoltaic and solar power forecasting for smart grid energy management," *CSEE Journal of Power and Energy Systems*, vol. 1, no. 4, pp. 38–46, 2015.
- [7] P. Gupta and R. Singh, "Pv power forecasting based on data-driven models: a review," *International Journal of Sustainable Engineering*, vol. 14, no. 6, pp. 1733–1755, 2021.
- [8] S. Aslam, H. Herodotou, S. M. Mohsin, N. Javaid, N. Ashraf, and S. Aslam, "A survey on deep learning methods for power load and renewable energy forecasting in smart microgrids," *Renewable and Sustainable Energy Reviews*, vol. 144, p. 110992, 2021.
- [9] D. Kaur, S. N. Islam, M. A. Mahmud, M. E. Haque, and Z. Y. Dong, "Energy forecasting in smart grid systems: recent advancements in probabilistic deep learning," *IET Generation, Transmission & Distribution*, vol. 16, no. 22, pp. 4461–4479, 2022.
- [10] G. Alkhatay and R. Mehmood, "A review and taxonomy of wind and solar energy forecasting methods based on deep learning," *Energy and AI*, vol. 4, p. 100060, 2021.
- [11] T. Capotosto, A. Rita Di Fazio, S. Perna, F. Conte, G. Iannello, and P. De Falco, "Day-ahead forecast of pv systems and end-users in the contest of renewable energy communities," in *2022 AEIT International Annual Conference (AEIT)*, 2022, pp. 1–6.
- [12] "Modelling and optimal management of renewable energy communities using reversible solid oxide cells," *Applied Energy*, vol. 334, p. 120657, 2023.
- [13] S. Chai, Z. Xu, Y. Jia, and W. K. Wong, "A robust spatiotemporal forecasting framework for photovoltaic generation," *IEEE Transactions on Smart Grid*, vol. 11, no. 6, pp. 5370–5382, 2020.
- [14] Y. Li, L. Song, S. Zhang, L. Kraus, T. Adcox, R. Willardson, A. Komandur, and N. Lu, "A tcn-based hybrid forecasting framework for hours-ahead utility-scale pv forecasting," *IEEE Transactions on Smart Grid*, 2023.
- [15] M. Bai, Y. Chen, X. Zhao, J. Liu, and D. Yu, "Deep attention convlstm-based adaptive fusion of clear-sky physical prior knowledge and multivariable historical information for probabilistic prediction of photovoltaic power," *Expert Systems with Applications*, vol. 202, p. 117335, 2022.
- [16] Ausgrid, "Solar home electricity data," 2014, [Online; Accessed 25-01-2023]. [Online]. Available: <https://www.ausgrid.com.au/Industry/Our-Research/Data-to-share/Solar-home-electricity-data>
- [17] A. Fentis, C. Lytridis, V. G. Kaburlasos, E. Vrochidou, T. Pachidis, E. Bahatti, and M. Mestari, "A machine learning based approach for next-day photovoltaic power forecasting," in *2020 Fourth International Conference On Intelligent Computing in Data Sciences (ICDS)*. IEEE, 2020, pp. 1–8.
- [18] D. Kaur, S. N. Islam, M. Mahmud *et al.*, "A vae-based bayesian bidirectional lstm for renewable energy forecasting," *arXiv preprint arXiv:2103.12969*, 2021.
- [19] —, "A bayesian deep learning technique for multi-step ahead solar generation forecasting," *arXiv preprint arXiv:2203.11379*, 2022.
- [20] M. Tortora, E. Cordelli, and P. Soda, "Pytrack: A map-matching-based python toolbox for vehicle trajectory reconstruction," *IEEE Access*, vol. 10, pp. 112 713–112 720, 2022.
- [21] O. Ltd., "Openweathermap," 2023, [Online; Accessed 25-01-2023]. [Online]. Available: <https://openweathermap.org>
- [22] "Global solar irradiance data and PV system power output data," <https://solcast.com>, 2019, [Online; accessed 2023-06-15].
- [23] A. Vaswani, N. Shazeer, N. Parmar, J. Uszkoreit, L. Jones, A. N. Gomez, E. Kaiser, and I. Polosukhin, "Attention is all you need," *Advances in neural information processing systems*, vol. 30, 2017.
- [24] J. Gehring, M. Auli, D. Grangier, D. Yarats, and Y. N. Dauphin, "Convolutional sequence to sequence learning," in *International conference on machine learning*. PMLR, 2017, pp. 1243–1252.
- [25] S. Hochreiter and J. Schmidhuber, "Long short-term memory," *Neural computation*, vol. 9, no. 8, pp. 1735–1780, 1997.
- [26] H. Song, D. Rajan, J. Thiagarajan, and A. Spanias, "Attend and diagnose: Clinical time series analysis using attention models," in *Proceedings of the AAAI conference on artificial intelligence*, vol. 32, 2018.
- [27] A. Dosovitskiy, L. Beyer, A. Kolesnikov, D. Weissenborn, X. Zhai, T. Unterthiner, M. Dehghani, M. Minderer, G. Heigold, S. Gelly *et al.*, "An image is worth 16x16 words: Transformers for image recognition at scale," *arXiv preprint arXiv:2010.11929*, 2020.
- [28] A. Baevski and M. Auli, "Adaptive input representations for neural language modeling," *arXiv preprint arXiv:1809.10853*, 2018.

- [29] A. Trask, D. Gilmore, and M. Russell, "Modeling order in neural word embeddings at scale," in *International Conference on Machine Learning*. PMLR, 2015, pp. 2266–2275.
- [30] K. Bayouhd, R. Knani, F. Hamdaoui, and A. Mtibaa, "A survey on deep multimodal learning for computer vision: advances, trends, applications, and datasets," *The Visual Computer*, pp. 1–32, 2021.
- [31] N. Srivastava, G. Hinton, A. Krizhevsky, I. Sutskever, and R. Salakhutdinov, "Dropout: a simple way to prevent neural networks from overfitting," *The journal of machine learning research*, vol. 15, no. 1, pp. 1929–1958, 2014.
- [32] F. Conte, S. Massucco, G.-P. Schiapparelli, and F. Silvestro, "Day-ahead and intra-day planning of integrated bess-pv systems providing frequency regulation," *IEEE Transactions on Sustainable Energy*, vol. 11, no. 3, pp. 1797–1806, 2020.
- [33] J. Zhang, X. Kong, J. Shen, and L. Sun, "Day-ahead optimal scheduling of a standalone solar-wind-gas based integrated energy system with and without considering thermal inertia and user comfort," *Journal of Energy Storage*, vol. 57, p. 106187, 2023.
- [34] F. Conte, S. Massucco, M. Saviozzi, and F. Silvestro, "A stochastic optimization method for planning and real-time control of integrated pv-storage systems: Design and experimental validation," *IEEE Transactions on Sustainable Energy*, vol. 9, no. 3, pp. 1188–1197, 2018.
- [35] N. E. Michael, S. Hasan, A. Al-Durra, and M. Mishra, "Economic scheduling of virtual power plant in day-ahead and real-time markets considering uncertainties in electrical parameters," *Energy Reports*, vol. 9, pp. 3837–3850, 2023.
- [36] A. Paszke, S. Gross, F. Massa, A. Lerer, J. Bradbury, G. Chanan, T. Killeen, Z. Lin, N. Gimeshe, L. Antiga *et al.*, "Pytorch: An imperative style, high-performance deep learning library," *Advances in neural information processing systems*, vol. 32, 2019.
- [37] D. P. Kingma and J. Ba, "Adam: A method for stochastic optimization," *arXiv preprint arXiv:1412.6980*, 2014.
- [38] J. Chung, C. Gulcehre, K. Cho, and Y. Bengio, "Empirical evaluation of gated recurrent neural networks on sequence modeling," in *NIPS 2014 Workshop on Deep Learning, December 2014*, 2014.
- [39] F. X. Diebold and R. S. Mariano, "Comparing predictive accuracy," *Journal of Business & economic statistics*, vol. 20, no. 1, pp. 134–144, 2002.